Comparison of Regularisation Methods in Image Reconstruction for Micro-Bioimpedance Tomography

Nadira Jamil, Yunjie Yang, Andreas Tsiamis, Jiabin Jia and Stewart Smith
School of Engineering
The University of Edinburgh
Edinburgh, United Kingdom.
n.jamil@ed.ac.uk

***Abstract*—Electrical impedance tomography (EIT) is an imaging technique that reconstructs the conductivity distribution of an inhomogeneous medium and is capable of monitoring physiological changes in biological materials. This paper focuses on comparison of state-of-the-art regularisation methods in solving the image reconstruction problem in micro-scale EIT for biomedical applications. Since the quality of image reproduction is weak for micro-scale phantoms, it is vital to study the image reconstruction algorithm. Hence, we present three regularisation methods in this paper - Tikhonov, Gaussian-Laplace and L_1 - for the image reconstruction of 700 µm diameter test samples. We verified our method using 500 µm × 250 µm rectangular Pt electrodes and compared the performance of these regularisation methods. The results suggest that Gaussian-Laplace regularisation provides better image reconstruction than L_1 and Tikhonov algorithms.**

Keywords— Tomography; image reconstruction; conductivity; microelectrodes; regularisation method

I. INTRODUCTION

Live-cell imaging is an important analytical tool in biomedical research and pharmaceutical laboratories. Live-cell microscopy involves a compromise between obtaining a good image quality and ensuring the cells are in a good condition. Hence, the spatial and temporal resolutions in an experiment are often limited to avoid exposing the cells to a high illumination intensity over a long period of time.

Electrical Impedance Tomography (EIT) is a promising technique for non-invasive, radiation-free, and conductivity-related process monitoring. It is widely relevant and safe for the patient, allowing real-time, continuous monitoring of electrical properties of organs or tissue over extended periods of time. EIT is a non-invasive imaging technique aiming to estimate conductivity distribution based on the calculated boundary voltages [1]. Tomography is an imaging technique performed by sectioning, through the use of any kind of penetrating wave. This technique is being applied in the field of biological [2] and physical sciences [3]. In most cases, the production of these images is based on mathematical tomographic reconstruction.

Fundamentally, EIT involves the solving of two problems: the forward problem and the inverse problem. The forward problem determines the electrical voltage distribution on the outermost surface of the phantom arising from the applied current pattern injection and conductivity distribution [4]. The inverse problem on the other hand is the image reconstructing step for EIT. The purpose of the reconstruction algorithm is to define conductivity distribution obtained from the electrical voltage measurement and sensitivity matrix [5].

There are a number of popular image reconstruction algorithms, including linear back-projection (LBP) [6], Landweber iteration [7], linear regularised Gauss-Newton method [8] and non-linear regularised Gauss-Newton method [8]. LBP is a simple and fast algorithm of image reconstruction, besides being one of the most common techniques used in electrical tomography [9]. It is regularly implemented for its high speed, however, it results in a low quality of reconstructed image. Therefore, to attain high-quality image reconstructions, iterative image reconstruction algorithms are applied and Landweber iteration is one of the examples [1]. It is based on the linearization of a normalised form of the problem.

In this paper, three regularisation methods in EIT image reconstruction are presented and compared for cell spheroid imaging using microelectrodes. The EIT system presented has the ability to produce high temporal resolution two-dimensional (2D) or three-dimensional (3D) images [10]. This extends the range of available live-cell imaging techniques, which are essential tools in biomedical research.

II. REGULARISATION METHOD

Theoretically, EIT defines the relationship between conductivity change, $\delta\boldsymbol{\sigma}$, and the potential difference, $\delta\mathbf{V}$, within a detecting domain. This relationship can be written as:

$$\delta\mathbf{V} = \mathbf{J}\delta\boldsymbol{\sigma} \tag{1}$$

where **J** is the Jacobian (sensitivity) matrix of EIT.

The image reconstruction for EIT encompasses the calculation of conductivity distribution when the current introduced is known and voltage readings are recorded. Due to the intrinsic ill-posedness and ill-conditioned characteristic of the EIT-image-reconstruction problem, the solution can be formulated as the following optimization problem based on regularisation techniques:

$$\delta\boldsymbol{\sigma}_\lambda = \arg\min_\sigma \|\mathbf{J}\delta\boldsymbol{\sigma} - \delta\mathbf{V}\|^2 + \lambda f(\delta\boldsymbol{\sigma}) \tag{2}$$

where λ represents the positive scalar regularisation parameter and f is the regularisation function encoding prior constraint information. The implementation of the various regularisation functions in (2) will be clarified in the next sub-sections.

We would also like to acknowledge the financial support of EPSRC (EP/K034510/1) IMPACT programme grant, People's Trust Council (Majlis Amanah Rakyat, Malaysia) and 2015 IEEE Instrumentation & Measurement Society Graduate Fellowship Award.

A. Tikhonov Regularisation

Tikhonov regularisation is one of the most popular regularisation methods for solving ill-posed inverse problems and has been applied to EIT image reconstruction. The Tikhonov regularisation can be generally formulated as:

$$\delta\boldsymbol{\sigma}_\lambda = \arg\min_\sigma \|\mathbf{J}\delta\boldsymbol{\sigma} - \delta\mathbf{V}\|^2 + \lambda\|\delta\boldsymbol{\sigma}\|^2 \quad (3)$$

Further, the solution of (3) can be written as:

$$\delta\boldsymbol{\sigma}_\lambda = (\mathbf{J}^T\mathbf{J} + \lambda\mathbf{I}^T\mathbf{I})^{-1}\mathbf{J}^T\delta\mathbf{V} \quad (4)$$

where **I** denotes the unity matrix.

B. Gaussian-Laplace Regularisation

Another commonly applied regularisation tool is the Gaussian-Laplacian method. Fig. 1 shows the three popular Laplacian operators applied to a single pixel. In this work, the first operator, i.e., the second-order four connected region Laplace operator, is adopted. Accordingly, Eq. (2) can be rewritten as:

$$\delta\boldsymbol{\sigma}_\lambda = \arg\min_\sigma \|\mathbf{J}\delta\boldsymbol{\sigma} - \delta\mathbf{V}\|^2 + \lambda\|\mathbf{L}\delta\boldsymbol{\sigma}\|^2 \quad (5)$$

Further, the solution of (5) can be written as:

$$\delta\boldsymbol{\sigma}_\lambda = (\mathbf{J}^T\mathbf{J} + \lambda\mathbf{L}^T\mathbf{L})^{-1}\mathbf{J}^T\delta\mathbf{V} \quad (6)$$

where **L** is the second-order four connected region Laplace operator matrix.

C. L_1 Regularisation

Over-fitting is a problem that occurs when a model contains a large set of data. Regularisation is one of the techniques to avoid over-fitting, where it 'pushes' the coefficients in, for example, vector, $\boldsymbol{x}$, to be zero for many components and then, reduces the vector size. L_1 regularisation is applied to the model to reduce its size. Hence, by implementing L_1 regularisation, vector $\boldsymbol{x}$ becomes smaller (more sparse), as most of the components are zeros.

Letting λ as the regularisation parameter, then Eq. (2) can be rewritten as:

$$\delta\boldsymbol{\sigma}_\lambda = \arg\min_\sigma \|\mathbf{J}\delta\boldsymbol{\sigma} - \delta\mathbf{V}\|^2 + \lambda\|\delta\boldsymbol{\sigma}\|_1 \quad (7)$$

Eq. (7) is solved iteratively based on the spectral projected gradient for L_1 minimization method [11].

III. Results and Discussions

The regularisation methods are verified by experiment to compare the performance of the methods described in Section II. The EIT sensor consists of 16 Pt electrodes microfabricated on a glass wafer [10]. The electrodes have identical dimensions of 500 µm × 250 µm and they are patterned around a 6 mm diameter circular probe area as shown in Fig. 2a.

Prior to the experiments, simulation using COMSOL Multiphysics 5.2a is performed for sensitivity analysis as depicted in Fig. 2b. In order to perform the time-difference imaging, the measurements are recorded twice; firstly to obtain calibration data from a homogeneous background (250 µL of phosphate-buffered saline (PBS) of concentration 1X), and then with a test sample with higher or lower conductivity. Fig. 3

0	1	0
1	-4	1
0	1	0

1	1	1
1	-8	1
1	1	1

-1	2	-1
2	-4	2
-1	2	-1

Fig. 1. Convolution kernels to approximate Gaussian-Laplace second-order derivates

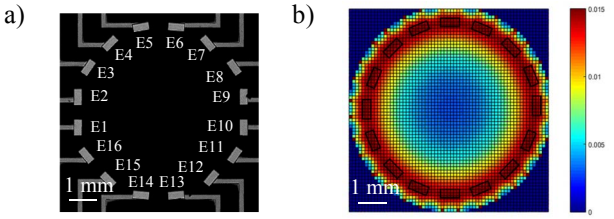

Fig. 2. a) Optical microscopy image of Pt microelectrodes and b) sensitivity distribution of 500 µm x 250 µm rectangular Pt electrodes. Colour bar scale denotes the normalized sensitivity ($\delta\mathbf{V}/\delta\boldsymbol{\sigma}$)

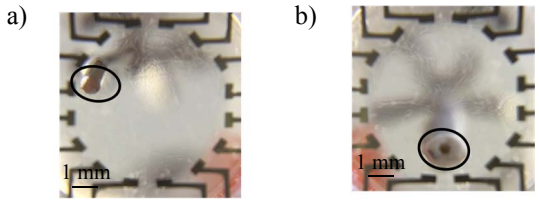

Fig. 3. a) Higher conductivity (copper metal) and b) lower conductivity (rubber) test samples. The positions of the test samples are indicated with black rings

shows the positions of the two test samples in relation to the microelectrodes.

The first measurement was performed with two pairs of electrodes. An alternating current of 1.5 mA was applied to the test sample through the first pair of electrodes, E1-E2, referring to Fig. 2 a) and voltage measurement was taken from the second pair of electrodes, E3-E4. The method was repeated and measurements were taken under 104 combinations of 16 electrodes. Each voltage measuring electrode pair gives different potential values based on the location of the imaged test sample. Fig. 4 presents three recorded data sets. The voltage difference range between 1 mV and 6 mV, and these graphs do not show large differences between each experiment. The patterns are regular in relation to the electrodes. If the setup is

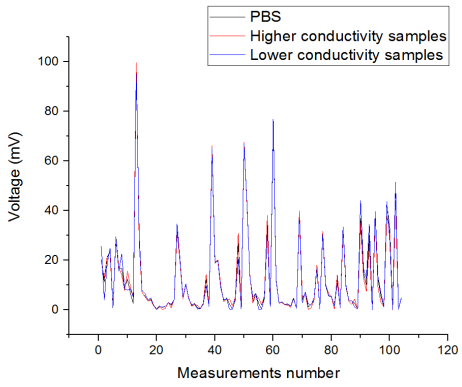

Fig. 4. (Black) Calibration data of phosphate-buffered saline (PBS), (red) measurement data with higher conductivity test samples, and (blue) lower conductivity test samples

TABLE I. IMAGE RECONSTRUCTIONS BASED ON DIFFERENT REGULARISATION METHODS (COLOUR SCALE IN Ω.CM)

Test sample	*Tikhonov Regularisation*	*Gaussian-Laplace Regularisation*	*L_1 Regularisation*
Higher conductivity	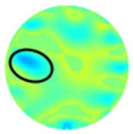	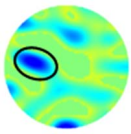	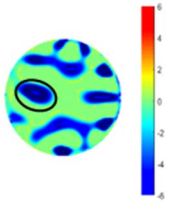
Lower conductivity		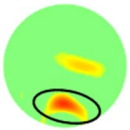	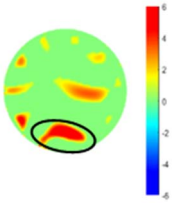

homogeneous, we should observe a regular pattern over 104 measurements. Therefore, the dissimilarities and irregular peaks observed in Fig. 4 are believed to be caused by the placement of the fluidic chamber and possible differences between electrodes. The peaks and variation are dependent on the fluidic chamber position, small changes in media volume and interfacial electrode impedance. Conductivity distribution is then estimated according to the potential variation obtained, and from the information gathered, image processing of the test sample can be implemented.

Calculations are performed based on the voltage difference values acquired and images are then reconstructed according to the three regularisation methods as shown in Table 1. For a test sample with higher conductivity, Tikhonov regularisation is unable to produce a high intensity image. Gaussian-Laplace regularisation gives the closest representation of the experiment setup although the intensity is not as high as L_1 regularisation. Although the reconstructed image is very strong using L_1 regularisation, errors also appear to be obvious. Ideally the background should not show significant variation in the conductivity.

Similar for a lower conductivity test sample, the best image reconstructed is produced by Gaussian-Laplace regularisation, despite having lower intensity as compared to L_1 regularisation as unwanted errors can be seen clearly in the image reconstructed using this technique.

IV. CONCLUSIONS

In this paper, we compared regularisation methods for solving EIT image reconstruction problems, particularly for cell spheroids imaging using microelectrodes. We have given an overview of three different regularisation methods, the issues that arise in these methods in relation to bio-impedance tomography and identifying the best regularisation method in image reconstruction of cellular activities. Gaussian-Laplace regularisation produces the most comparable image with the experimental setup. Reconstructed images using L_1 regularisation on the other hand have the highest intensity, although the presence of unwanted errors is noticeable.

ACKNOWLEDGMENT

The authors would like to acknowledge the assistance of Mr. Iain Gold and Mr. Kevin Tierney with PCB fabrication.

REFERENCES

[1] Zhang, L. (2011) Image reconstruction algorithm for electrical impedance tomography using updated sensitivity matrix. 2011 International Conference of Soft Computing and Pattern Recognition (SoCPaR), Dalian, pp. 248-252.

[2] Armen, R. K. et al. (2008) A review of imaging techniques for systems biology, BMC Systems Biology, 2:74.

[3] Midgley, P. A., & Weyland, M. (2003). 3D electron microscopy in the physical sciences: the development of Z-contrast and EFTEM tomography. Ultramicroscopy, 96(3-4), 413 - 431.

[4] Wang, Q. & Wang, H. (2011) Image reconstruction based on 11 regularization for electrical impedance tomography (EIT) in Instrumentation and Measurement Technology Conference (I2MTC).

[5] Borcea, L. (2002) Electrical impedance tomography. Inverse problems. 18(6): p. R99 – R136.

[6] Lei, J. et al. (2009) An image reconstruction algorithm based on the extended Tikhonov regularization method for electrical capacitance tomography, Measurement, Volume 42, Issue 3, April, Pages 368-376.

[7] Yang, W. Q. et al. (1999) "An image reconstruction algorithm based on Landweber's iteration method for electrical-capacitance tomography," Measurement Science and Technology, vol. 10(11), p.1065.

[8] Stephenson, D. R. et al. (2005) Comparison of 3D Image Reconstruction Techniques using Real Electrical Impedance Measurement Data 4th World Congress on Industrial Process Tomography, Aizu, Japan.

[9] Kotre, C.J., (1989) A sensitivity coefficient method for the reconstruction of electrical impedance tomograms, Clin. Phys., Physiol. Meas., 10, pp. 275-281.

[10] Jamil, N. et al. (2016) Design and fabrication of microelectrodes for electrical impedance tomography of cell spheroids. IEEE EMBS Conference on Biomedical Engineering and Sciences (IECBES 2016). Kuala Lumpur, Malaysia. pp. 426-431.

[11] Van Den Berg, E., & Friedlander, M. P. (2008). Probing the Pareto frontier for basis pursuit solutions. *SIAM Journal on Scientific Computing*, *31*(2), 890-912.